COBRA-SFS DRY CASK MODELING SENSITIVITIES IN HIGH-CAPACITY CANISTERS*

Remy Devoe and Kevin R. Robb

Oak Ridge National Laboratory, P.O. Box 2008, MS-6170, Oak Ridge, TN 37931, USA devoer@ornl.gov

Material temperature predictions for dry-cask storage are dependent to varying degrees on user specified model assumptions. To understand the importance of various areas of the dry-cask thermal model, the temperature prediction sensitivity of these parameters has been evaluated. Thermal modeling assumptions are used to approximate cask geometry, fuel assembly design variations, physical properties of cask materials and fill-gas, and environmental conditions of the storage site. The result of this sensitivity study identifies which of these areas will produce the largest reduction in temperature prediction uncertainty with additional testing and measurements of actual cask systems. The scope of this work is to understand the COBRA-SFS modeling parameter sensitivities for the vertical high-capacity canister system. In general, the results show that cask material temperatures depend most on radiative and convective heat transport. The accuracy of the COBRA-SFS model for high-capacity vertical canisters hinges upon accurately modeling channel geometry in the canister and cask annulus.

I. INTRODUCTION

High-capacity canisters are anticipated to be the most widely used design at independent spent fuel storage installations (ISFSIs) because of the reduced storage cost per assembly. Burnup credit in criticality analyses is in part responsible for increased capacity in dry casks, but concerns over criticality safety have always been accompanied by thermal limitations. Canisters with increased capacity sizes inherently come with a higher thermal loading to be rejected via passive systems to the environment. The average time between reactor discharge and loading of fuel in dry-casks is also lower as a result of older fuel having already been loaded in dry-casks. UNF storage canisters rely on natural convective, radiative, and conductive heat transfer mechanisms to passively reject decay heat to the environment. High-capacity canisters reject heat primarily through natural convection and radiative heat transport to the canister shell. Because both modes depend on temperature gradient to varying extents, modeling and simulation of the unique passive heat removal systems that reject heat from dry casks is an active area of research for safety and integrity monitoring.

I.A. Background

Dry-cask thermal models for this project are incorporated as a part of the UNF-Storage Transport & Disposal Analysis Resource and Data System (UNF-ST&DARDS), which uses an integrated database of UNF inventory data to analyze dry-cask performance in terms of dose, criticality, and temperature [1]. Reliable thermal models using the Coolant-Boiling in Rod Arrays-Spent Fuel Storage (COBRA-SFS) code package [2] produce expedient low-uncertainty temperature predictions to meet these assessment capabilities. COBRA-SFS is used to characterize material temperatures during both steady-state and transient conditions encountered during loading, storage, and transportation operations. The temperature predictions are used for informing material degradation studies and meeting regulatory criteria for transportation.

I.B. Objectives

Main objectives of this study are to develop a suite of modeling options for dry-cask thermal characterization that includes evaluating the best-estimate, bounding-high, and bounding-low temperature predictions. Best-estimate modeling assumptions utilize the best available data and modeling practices to produce realistic temperature predictions. Typically, for licensing purposes all modeling assumptions are on a bounding-high basis. This conservatism in thermal models for canister design licensing does not lend itself to evaluating best-estimate temperatures. Bounding-low temperature modeling assumptions are just the opposite and use realistic configurations that would produce lower than best-estimate temperature predictions. This modeling option is important to determining when the ductile-to-brittle transition occurs in cladding during storage.

I.C. Approach

The modeling options for best-estimate, bounding-high, and bounding-low temperature predictions are determined through a parametric study of canister and assembly COBRA-SFS modeling characteristics. A model developed from the MAGNASTOR transportable storage container (TSC) for pressurized water reactor (PWR) fuel is used as the base case for the study. Each parameter in this study is individually perturbed from the base-case model to observe the effect on peak cladding temperature (PCT). PCT is the chosen observable for the study since all other material temperatures are dependent upon the temperature of the cladding. The maximum decay heat loading for a uniform loading and a preferential loading configuration was used in all cases.

I.D. Tools and Capabilities

The thermal analysis code package COBRA-SFS is used to evaluate the thermal performance of the canister system. COBRA-SFS is a sub-channel based analysis code that was specifically designed for UNF storage casks and transport packages in which there is no two-phase flow. COBRA-SFS has a rich validation history including pre- and post- test comparisons against tests with single fuel assemblies [3, 4] and casks containing multiple assemblies [5, 6]. The validation base includes various cask designs, assembly types and powers, backfill gases, and canister orientations. COBRA-SFS models individual pins in each assembly and the flow through each sub-channel formed between the pins and around the assembly in each basket position. The grey-body view factors used to calculate radiative heat transport are generated using the stand-alone code RADGEN, which is made available with COBRA-SFS. The output of COBRA-SFS includes each slab axial position temperature, the temperature of the fluid in each channel by axial position, and the mass flow rate of the fluid in each channel. The output is used in VisIt [7] to generate temperature and flow rate maps of the canister basket. Components of the input file are automatically generated with the COBRA-Creator Of Most Assembly's Necessary Data, Even RADGEN (COBRA-COMANDER) tool [8]. This tool has data libraries for assembly and cask type designations which are used to construct assembly and basket channels and rod arrays. RADGEN is also run for each type of assembly stored in the canister to generate specific view factors for each rod.

II. MODEL DEVELOPMENT

The COBRA-SFS base-case model is of the NAC Int. MAGNASTOR TSC-37. The MAGNASTOR storage cask contains many similarities to the other high-capacity cask systems. This includes an egg-crate basket design with closely spaced fuel assemblies and no heat conduction plates. The TSC holds up to 37 PWR assemblies and is welded shut after loading. The canister is in a transfer over-pack during loading, which provides shielding while the canister is loaded into a concrete storage over-pack or transport over-pack. The base-case model is for steady-state in the storage over-pack with explicit modeling of assemblies, basket structural components, TSC shell, cask annulus, over-pack geometry, and associated upper and lower plenums. Realistic bounding parameters are chosen on the basis of PCT results taking into consideration factors that would lead to that configuration.

II.A. Summary Model Description

The fuel basket consists of 21 fuel tubes welded together at the corners to create 16 developed cells. The developed cells consist of four fuel tubes or three fuel tubes and the basket support weldment on the fourth side. Together the fuel tubes and developed fuel cells form a regular grid patterned basket. The fuel basket resides inside a sealed stainless steel canister. The canister rests on a pedestal and is surrounded by a concrete over-pack. The annular region between the canister and concrete over-pack provides air flow to cool the canister.

II.A.1. MAGNASTOR Cask Geometry

The storage over-pack has an inner carbon steel wall and an outer thick reinforced concrete wall. The over-pack is divided uniformly radially and circumferentially into nodes that are connected to adjacent nodes and channels. The over-pack has four air inlets and exits around the base plate and lid to allow ambient air to flow up the cask annulus and remove heat from the canister. Figure 1 illustrates the basket, support structure, and over-pack discretization of the base-case model.

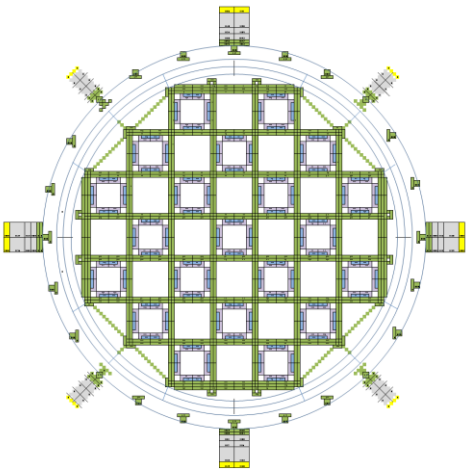

Fig. 1. Cask nodalization of the base-case model.

The inside walls of the fuel tube are lined with a neutron absorber plate encased in a stainless steel sheet. These absorbers act as a means of criticality control and are included in the thermal model. Each fuel tube is constructed of carbon steel with carbon steel weld rods on each corner to connect the tubes to one another. The basket region is divided axially into 47 nodes to capture temperature variations along the length of the container. The fuel tube nodalization is illustrated in Fig. 2.

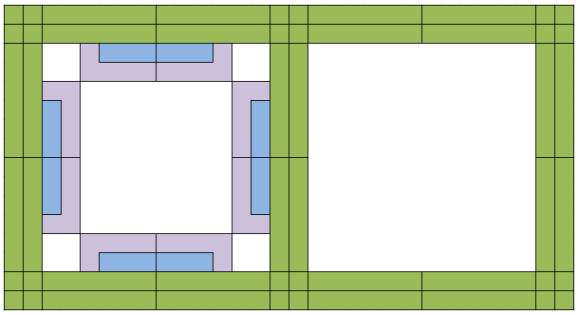

Fig. 2. Fuel tube and developed cell node scheme.

II.A.2. Assembly Geometry

The fuel used for the base-case model is Westinghouse 15 × 15 LOPAR fuel. The fuel is modeled with 204 fuel rods, 21 thimble tubes, and 256 sub-channels as shown in Fig. 3. The rod and thimble diameters are 0.422 in. and 0.482 in., respectively, with a pin pitch of 0.563 in. The base-case model includes seven spacer grids and the lower and upper end-fitting with a form loss of 2.0 for each spacer grid and 0.5 for the end-fittings. The cladding is modeled as Zircaloy using emissivity data consistent with thick oxide layer formation.

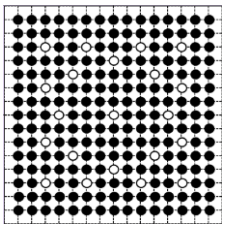

Fig. 3. Westinghouse 15 × 15 LOPAR fuel.

II.A.3. Materials

Material properties for the cask components in the base-case model are obtained from the MAGNASTOR Safety Analysis Report (SAR) [9]. The material properties are listed in Table I. Temperature-dependent gas properties for air at 1 atm and helium at 7 atm were taken from the National Institute of Standards and Technology (NIST) fluid properties database.

TABLE I. Material Properties

Material	Thermal conductivity (Btu/h-ft-°F)	Emissivity (–)
Stainless Steel 304	$4.82+0.0078*T-2E-06*T^2$	0.36
Carbon Steel 537	$24.51+0.0113*T-1E-05*T^2$	0.8
Neutron Absorber	61.3	0.15
Aluminum 110	$173.22-0.1062*T+6E-05*T^2$	0.36
Concrete	0.708	0.8
Earth	0.347	–
Cladding	8.71	0.8

II.B. Comparison Results

The base-case model uses design drawings from the MAGNASTOR SAR to infer geometry and material specifications. To verify the validity of the model, test cases are compared to test case results reported in the SAR. These include various assembly loading variations and a no-heat simulation in which only environmental factors affect the temperature profile of the cask. These tests are used as a quality control to ensure the base-case model performs as expected.

II.B.1. Case Scenario and Modeling Assumptions

Two loading pattern variations were considered: a uniform loading pattern and a preferential loading pattern. Each variation used the maximum assembly decay heat allowed for loading. A separate study for long cooling times would require modeling decreased decay heat over time. For uniform heat loading, the assembly power is 0.959 kW. For preferential heat loading, there are three zones with maximum decay heat values of 0.8 kW, 1.2 kW, and 0.922 kW for regions A, B, and C respectively. The preferential loading pattern is shown in Fig. 4.

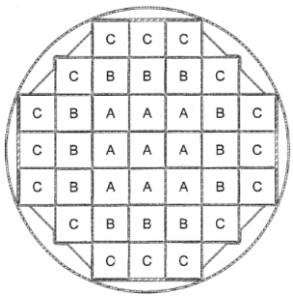

Fig. 4. Preferential decay heat loading zones.

For the sensitivities presented the base-case model uses the uniform loading pattern. No significant differences were observed when selected sensitivities using the preferential loading pattern were compared against the base-case (uniform loading) results. The base-case model assumes an ambient air temperature of 80 °F and a 12-hour average solar insolation of 61.46 Btu/h-ft^2 and 122.9 Btu/h-ft^2 for the side and top boundary conditions, respectively. The ground temperature is assumed to be 40 °F. The burnup profile in Fig. 5 is taken from the PWR axial profile database [10] and represents the nominal profile across all burnups, enrichments, and fuel designs. Assembly axial power profiles are divided into 18 positions.

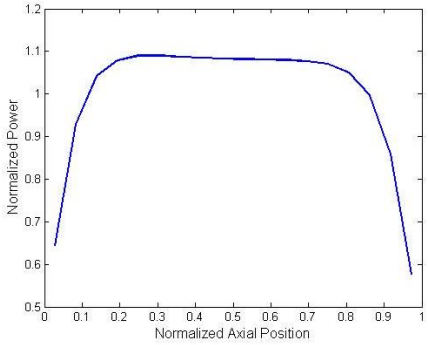

Fig. 5. Base-case assembly axial profile.

The pressure drop in the annulus region due to buoyancy-driven circulation is 0.0074712 psi based on the height of the heated column of air in the annulus. The gap between the structural components and the TSC shell is assumed to be 0.125 in., which is the tolerance on the design diagram dimensions for basket components.

II.B.2. Base-Case Verification

Two simulations are evaluated to determine the maximum cladding temperature using the base-case model. The cases are for ambient temperatures of -40 °F and 106 °F. The MAGNASTOR SAR results for this simulation and the base-case model are shown in Table II.

TABLE II. Peak Cladding Temperature Results (°F)

Air Temperature	SAR Peak (°F)	Base-Case Peak (°F)
-40	617	578
106	756	729

Results of the simulation indicate that the base-case model is under-predicting the results from the MAGANASTOR SAR. There are major differences in modeling assumptions between the SAR analysis and the base-case, namely that the SAR model is a 2-D finite element model of the maximum temperature plane. The base-case model averages the temperature of each node over an axial discretization of 3.5 in. For a smaller discretization, PCT will increase as the average temperature of each node will be closer to the PCT within that node. The SAR model also uses gaps between the welded tie-rod and fuel tube and neglects conduction to the canister shell entirely. The base case was modified to neglect conduction to the canister shell.

III. COBRA-SFS MODEL SENSITIVITIES

Many assumptions are used to generate thermal models, and some of these assumptions have been discussed in the description of the base-case model for the MAGNASTOR TSC-37 storage cask. To determine the impact of these assumptions on model reliability, these parameters are tested for PCT sensitivity by using a range of values that one could expect to see in storage operations.

III.A. Assembly Model Parameters

UNF assembly data has some of the widest ranges of unknowns for dry-cask analysis. Data provided in the RW-859 forms indicate the assembly design, initial enrichment, burnup, and discharge date, but cycle history information is not included. Cycle history has a significant impact on isotopic inventory uncertainty. The effect of isotopic inventory uncertainty on temperature prediction for the first 100 years is assumed to be negligible. This is because decay heat in this time period is dominated by fission product activity which depends directly on burnup. For long-term (>100 years) thermal modeling, sensitivity to irradiation history will be significant because the actinide compositions will dominate the thermal source term. This study only focuses on the assembly parameters that affect the COBRA-SFS model, namely burnup profile, cladding emissivity, and spacer-grid drag coefficients.

III.A.1. Burnup Profile

Burnup profile data is grouped into 5 GWd/MTU burnup bins to evaluate the effect of burnup on profile shape. It has been determined from a scoping study that using a top-heavy profile (more than half the assembly power is produced in the top half) reduces natural circulation flow in the canister. The reduced mass flow rate reduces convection and increases PCT. Conversely, a profile that is bottom-heavy reduces PCT. Bounding hot and cold burnup profiles are shown in Figs. 6. Each burnup heat loading is 959 W to compare profile shape sensitivity. In reality, lower burnup fuel would have a much lower decay heat, minimizing the observed effect. These profiles are used in the base-case model to produce

the bottom graph in Fig 6. The bounding profiles are chosen on the basis of an algorithm that searches for the highest and lowest top to bottom integrated power ratio and resulted in the profiles shown in Fig. 6. For lower burnups the difference between nominal and bounding hot and cold is much greater than for medium to high burnup. This indicates a more uniform power distribution in fuel as burnup increases. The maximum difference between nominal and the bounding case is 13 °C or 2.04% for burnup below 15 GWd/MTU.

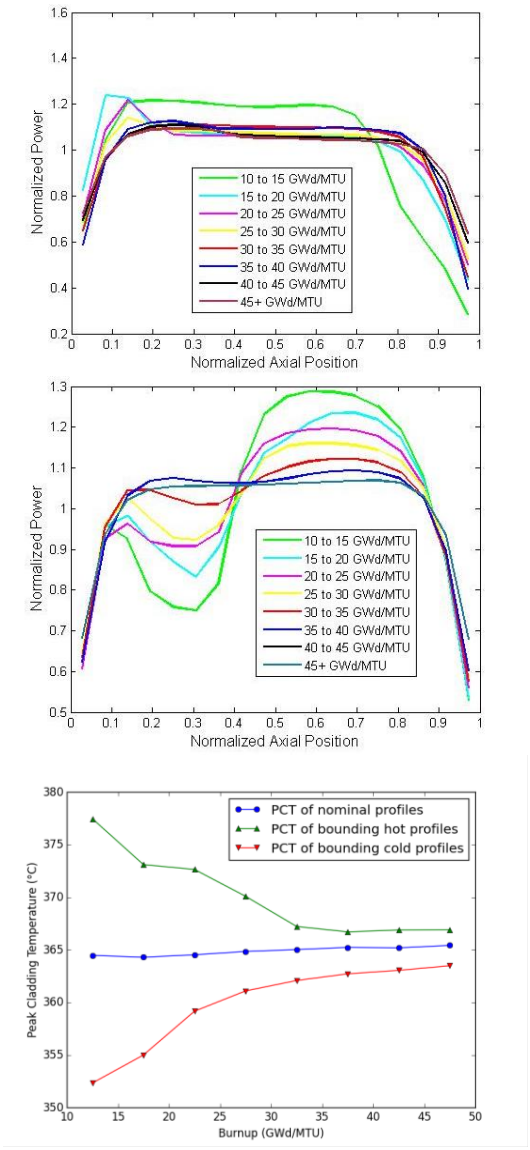

Fig. 6. Bounding hot (top) and cold (middle) profiles and PCT results (bottom).

III.A.2. Cladding Emissivity

Cladding emissivity can vary greatly owing to material type (Zircaloy or stainless steel), oxide layer thickness, crud deposition, and other chemical reactions on the surface of the cladding. The emissivity is varied from the base-case value of 0.8 to 0.3 (Table III). This represents the range of emissivity variation for clean stainless steel and thick oxide layer formation [11]. PCT increased with lower emissivity due to lower radiative heat transfer from the rods. The maximum change in PCT between 0.8 and 0.3 was 2.7 °C or 0.42%, showing that rod emissivity has low impact in terms of temperature prediction sensitivity.

TABLE III. Rod Emissivity Results

Rod Emissivity	PCT (°C)	Difference (%)
0.8	364.8	0.00%
0.7	365.4	0.09%
0.6	365.9	0.17%
0.5	366.5	0.26%
0.4	367.0	0.34%
0.3	367.5	0.42%

III.A.3. Assembly Component Drag Losses

The seven spacer grids and the inlet and outlet drag coefficients on the basket have the effect of decreasing the mass flow rate of gases recirculating within the canister. Having a higher form loss for these obstacles would increase PCT due to lower convective heat transfer. The form loss for each spacer-grid is varied from the base-case value of 2 to 100, and the PCT results are plotted in Fig 7.

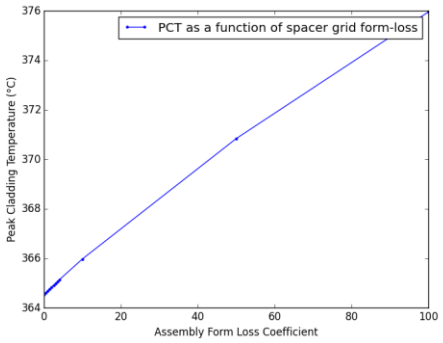

Fig. 7. Spacer-grid form loss variation results.

A value of 2 is characteristic of grids while the maximum value of 100 was chosen as a high value in order to evaluate the trend. The maximum temperature difference from the base-case model for a loss coefficient of 100 is 11 °C or 1.74%. For blocked flow in the basket channels, PCT rises 137 °C or 21.53%.

III.B. Cask Model Parameters

The base-case MAGNASTOR TSC-37 model was created with information from licensing documentation. A number of assumptions not explicitly detailed in the SAR were used in the creation of the base-case model. The uncertainty in predictions from using these modeling assumptions is related to the sensitivity of these assumed parameters.

III.B.1. Gap Conduction

The gaps between two materials are modeled by specifying a resistance that impedes conduction between the two materials. Gaps can range from the material surface roughness and to as large as inches. Gaps that are very large (>1/2") usually also have convective gas flow and should be modeled as a channel instead. All gaps include radiative heat transfer between the materials. Gap size depends on thermal expansion in the basket, which means that a rigorous model would require iterative runs to converge both gap size and resulting temperature predictions. The gap size also varies due to tolerances in the manufacturing process. The size of the gap between the shell and basket corners was varied from 0 inch to 1 inch to determine the effect on PCT. The PCT results for various gaps sizes are plotted in Fig. 8.

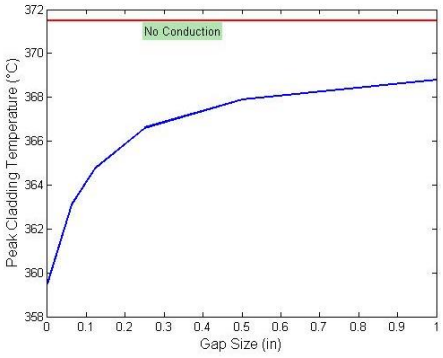

Fig. 8. Gap width in shell–basket conduction.

The base-case uses a conduction gap of 0.125 in., and the maximum 1 in. conduction gap studied results in an increase of 4 °C or 1%. In the case that conduction to the canister shell is completely neglected as is in the SAR, the PCT rises 6.6 °C or 1.04% indicating that conduction to the canister shell is a minor pathway for heat removal for this canister design.

III.B.2. Fill-Gas Pressure

The canister is required to be back-filled after drying with helium gas to an internal gauge pressure of 7 atm. Pressurizing helium increases density and, therefore, natural circulation and conductivity. Results for the base-case model using varying pressurizations are shown in Fig. 9. The gas pressure has a significant effect on PCT, so leakage over time can reduce pressure to levels below 7 atm, resulting in possibly higher cladding temperatures depending on the age of the fuel. For atmospheric pressure the base-case PCT rises by 26% to 531 °C, violating licensing temperature limits.

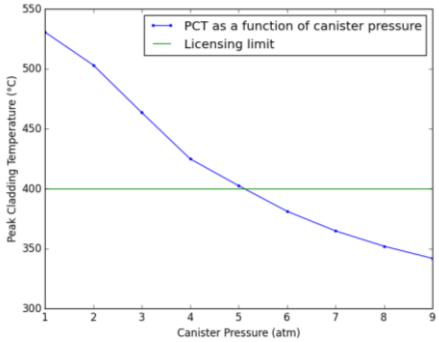

Fig. 9. Canister fill-gas pressure effects on PCT.

III.B.3. Material Properties

Material properties in the base-case model were taken from the SAR thermal modeling sections. These values were compared to those found in open literature, and the greatest difference was 15.5% in conductivity. All solid material conductivities are modeled in the base case ± 15.5% with results listed in Table IV. Both cases exhibit only a maximum 2.6 °C change in PCT, which shows that material temperature predictions are not very sensitive to changes in conductivity. These results are expected given the low PCT sensitivity to conduction gap size.

TABLE IV. Material Property Results

Material Conductivity (%)	PCT (°C)	Difference (%)
84.5%	362.4	-0.38%
100.0%	364.8	0.00%
115.5%	367.4	0.41%

III.B.4. Annulus Pressure Head

The pressure drop drives flow in the air annulus between the canister and cask over-pack is hard-coded into each simulation. The pressure drop is due to buoyancy forces that drive the higher temperature therefore lower density air in the annulus out the exit vent and allows cooler air to enter at the base of the cask. The pressure head is proportional to the height between the air inlets and outlets of the over-pack and the difference in the two air densities. COBRA-SFS uses the average air density in the annulus channel region to determine the

buoyancy force, but does not take into account the heated air in the upper plenum of the annulus as shown in Fig 10. The user must include the height of the basket region, the form loss of the exit vent, and additional height of heated air in the upper plenum to calculate the pressure drop.

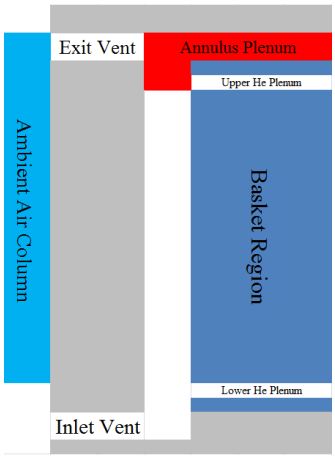

Fig. 10. Dry-cask annulus and plenum diagram.

Multiple selections of pressure head are simulated to determine the sensitivity of PCT predictions to annulus pressure head. These results are listed in Table V. The base case uses the height from the basket bottom to the annulus exit vent in ambient air minus the heated air column in the annulus upper plenum. The bounding hot model uses only the basket region height, which produces a PCT of 369.2 °C, an increase of only 0.8%. The bounding cold model uses the height from inlet vent to exit vent, which reduces PCT from the base-case model by 6.6%.

TABLE V. Annulus Pressure Head

PSIA (lb/in.^{2})	PCT (°C)	Difference (%)
0.0069915	369.2	0.69%
0.0070774	364.8	0.00%
0.0075899	345.1	-3.09%
0.0082618	329.4	-5.55%

III.B.5.Basket Emissivity

Radiative heat transport is crucial to removing heat from the canister and fuel stored within. A number of simulations were run in which radiative heat transfer was not incorporated in all or portions of the model (Table VI). The results of these simulations show where radiative heat transport is most important. Without any radiative heat transport, PCT rises 18.59% to 483 °C. The results show that radiative heat transport is most important between the basket support structure and the canister shell, which when not accounted for increases the PCT by 16.82%. There is also significant heat removal through radiative heat transfer from the canister's exterior to the over-pack inner liner. The over-pack inner liner is heated by radiated heat from the canister shell, in effect doubling the convection surface area within the annulus.

TABLE VI. Radiative Heat Transfer Sensitivity Results

Test Case	PCT (°C)	Difference (%)
Base Case	364.8	0.00%
No Radiation	483.4	18.59%
No Basket-Canister	472.1	16.82%
No Rod-Rod and Rod-Basket	372.2	1.16%
No Annulus	395.1	4.75%

III.C. Environmental Factors

The environment around ISFSIs has more variability than many of the sensitivities studied inside the canister. Ambient air temperatures, annulus pressure head, and insolation are used as the boundary conditions for the problem. The sensitivity of the COBRA-SFS model to these variables is explored in the following section. Other factors such as wind, air humidity, and annulus vent blocking are not modeled and were not investigated.

III.C.1. Ambient Air Temperature

The ambient air temperature affects many factors in the COBRA-SFS model. The boundary conditions of natural convection on the side and top of the over-pack must be changed to the new bulk air temperature. The pressure drop in the annulus must also change to account for the change in air density. Figure 11 shows that PCT is linearly proportional to ambient air temperature. PCT will decrease or increase by the same difference as the ambient air temperature. This makes PCT highly sensitive to ambient air temperature.

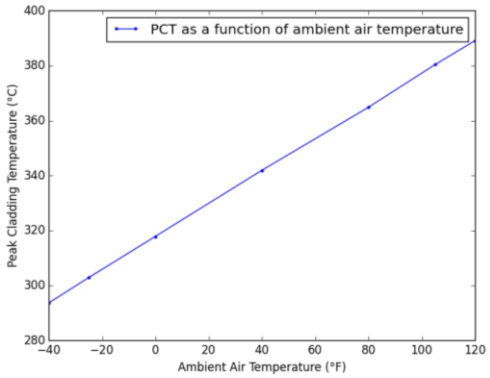

Fig. 11. Ambient air temperature effects on PCT.

III.C.2. Insolation

The COBRA-SFS base-case model uses a daily average insolation on the top and sides of 122.9 and 61.46 Btu/h-ft^2. The top is twice that of the sides because of shadowing as the sun moves from one side of the cask to the other. The average insolation for the United States is less than half that of the base-case assumption. Using nominal geographic insolation data will produce significantly less variation in PCT. The difference between the base-case model and the no solar insolation PCT is less than 1 °C (Table VII), which shows that PCT not very sensitivity to solar insolation. The canister temperatures change little with insolation because the over-pack is thermally isolated from the canister due to buffering from air in the annulus.

TABLE VII. Insolation Effects

Side	Top	PCT (°C)
On	On	364.71
On	Off	363.91
Off	On	365.21
Off	Off	364.34

IV. CONCLUSIONS

The most significant variations in PCT in COBRA-SFS modeling parameters are for fill-gas pressure, annulus pressure head, ambient air temperature, and radiative heat transfer. Over the range of parameters investigated, the maximum variations in PCT observed are provided in Table VIII. The results show that temperature predictions are most sensitivity to the modeling specifications that determine convective and radiative heat transfer properties. It should be noted that the sensitivity results are applicable within the range of the parameters investigated and care should be taken when extrapolating the results to different conditions.

TABLE VIII. Results Summary

Sensitivity	Δ PCT (°C)	Difference (%)
Burnup Profile	13	2.04
Rod Emissivity	2.7	0.42
Spacer Grid	11	1.74
Shell-Basket Gap	6.6	1.04
Fill-gas Pressure	166	26.0
Material Conductivity	2.6	0.41
Annulus Pressure Drop	-35.4	-5.6
Ambient Air Temperature	-128	-13.3
Basket Emissivity	119	18.6
Insolation	-0.89	-0.14

ACKNOWLEDGMENTS

Special thanks to John Scaglione, Rob Lefebvre, Paul Miller, and Steve Skutnik for their contributions to this project. Research supported by the DOE Office of Used Nuclear Fuel Disposition Research and Development and the Nuclear Fuels Storage and Transportation Planning Project.

REFERENCES

1. J. Peterson, *Used Nuclear Fuel Storage, Transportation & Disposal Analysis Resources and Data System (UNF-ST&DARDS),* FCRD-NFST-2013-000117 Rev. 0, Oak Ridge National Laboratory, Oak Ridge, TN, March 2013.
2. Pacific Northwest Laboratory, *COBRA-SFS Cycle 3: Code System for Thermal Hydraulic Analysis of Spent Fuel Cask*, RSICC Code Package PSR-72 (2003).
3. N. J. Lombardo, T. E. Michener, C. L. Wheeler, D. R. Rector, "COBRA-SFS Predictions of Single Assembly Spent Fuel Heat Transfer Data," PNL-5781, April 1986.
4. J. M. Cuta, J. M. Creer, "Comparisons of COBRA-SFS Calculations With Data From Simulated Sections of Unconsolidated and Consolidated BWR Spent Fuel," NP-4593, August 1986
5. L. E. Wiles, N. J. Lombard, C. M. Heeb, U. P. Jenquin, T. E. Michener, C. L. Wheeler, J. M. Creer, R. A. McCann, "BWR Spent Fuel Storage cask Performance Test, Volume II Pre- and Post-Test Decay Heat, Heat Transfer, and Shielding Analysis," PNL-5777 Vol. II, June 1986.
6. M. A. McKinnon, D. P. Batalo, D. H. Schoonen, et. al., "The MC-10 PWR Spent-Fuel Storage cask: Testing and Analysis," EPRI NP-5268, PNL-6139, July 1987.
7. H. Childs, et al., "VisIt: An End-User Tool For Visualizing and Analyzing Very Large Data," High Performance Visualization--Enabling Extreme-Scale Scientific Insight, pg 357-372, Oct. 2012.
8. K. R. Robb, *COBRA-COMANDER cycle 1.0, Input Generator for COBRA-SFS*, ORNL/TM–2014/9, March 2014.
9. NAC International, *MAGNASTOR Final Safety Analysis Report*, Docket No. 72-1031 (2010).
10. R. J. Cacciapouti and S. Van Volkinburg, *Axial Burnup Profile Database for Pressurized Water Reactors*, YAEC-1937, Yankee Atomic Electric Company (1997).
11. L. J. Siefken, E. W. Coryell, E. A. Harvego, J. K. Hohorst, *A Library of Materials Properties for Light Water-Reactor Accident Analysis*, NUREG/CR-6150 (2001).